Thermal properties of asymmetric nuclear matter with an improved isospin- and momentum-dependent interaction

Jun Xu,[1,2,*] Lie-Wen Chen,[3,4,†] and Bao-An Li[5,6,‡]

[1]*Shanghai Institute of Applied Physics, Chinese Academy of Sciences, Shanghai 201800, China*
[2]*Kavli Institute for Theoretical Physics, Chinese Academy of Sciences, Beijing 100190, China*
[3]*Department of Physics and Astronomy and Shanghai Key Laboratory for Particle Physics and Cosmology, Shanghai Jiao Tong University, Shanghai 200240, China*
[4]*Center of Theoretical Nuclear Physics, National Laboratory of Heavy Ion Accelerator, Lanzhou 730000, China*
[5]*Department of Physics and Astronomy, Texas A&M University-Commerce, Commerce, TX 75429-3011, USA*
[6]*Department of Applied Physics, Xi'an Jiao Tong University, Xi'an 710049, China*

arXiv:1410.1604v2 [nucl-th] 10 Jan 2015

Thermal properties of asymmetric nuclear matter, including the temperature dependence of the symmetry energy, single-particle properties, and differential isospin fractionation, are investigated with different neutron-proton effective mass splittings using an improved isospin- and momentum-dependent interaction. In this improved interaction, the momentum-dependence of the isoscalar single-particle potential at saturation density is well fitted to that extracted from optical model analyses of proton-nucleus scattering data up to nucleon kinetic energy of 1 GeV, and the isovector properties, i.e., the slope of the nuclear symmetry energy, the momentum-dependence of the symmetry potential, and the symmetry energy at saturation density can be flexibly adjusted via three parameters x, y, and z, respectively. Our results indicate that the nucleon phase-space distribution in equilibrium, the temperature dependence of the symmetry energy, and the differential isospin fractionation can be significantly affected by the isospin splitting of nucleon effective mass.

PACS numbers: 21.65.-f, 21.30.Fe, 24.10.Pa, 64.10.+h

I. INTRODUCTION

Understanding the in-medium nucleon-nucleon (NN) interaction is one of the main tasks of nuclear physics. The single-particle potential of a nucleon in nuclear medium is closely related to the NN interaction as well as the properties of nuclear matter. Based on the Brueckner theory, the potential of a nucleon depends not only on the properties of the medium but also on the momentum of the nucleon, and the momentum dependence comes from the exchange contribution of the finite-range NN interaction within Hartree-Fock framework. More than twenty years ago, for studying heavy-ion collisions the momentum-dependent mean-field potential was gradually improved from the Gale-Bertsch-Das Gupta (GBD) interaction [1] to a momentum-dependent Yukawa interaction (MDYI) [2, 3]. Later, the isospin-dependence was further introduced to the momentum-dependent potential and the newly developed interaction is named as MDI [4]. It has been found that the momentum dependence of the nucleon potential affects not only the dynamics of heavy-ion collisions (see Ref. [5] for a review) but the thermodynamical properties of nuclear matter as well [6, 7]. This interaction has further been used to study the core-crust transition density of neutron stars [8–10] and study the properties of hybrid stars after it was extended to include hyperon interactions [11]. Moreover, the MDI interaction together with an isospin-dependent Boltzmann-Uehing-Uhlenbeck transport model was used to study the symmetry energy at both subsaturation [12] and suprasaturation densities [13]. For a latest review of the MDI interaction, we refer the readers to Ref. [14].

The above MDI interaction was further improved in 2010 [15], and the new interaction, dubbed ImMDI, mainly includes the following three improvements. First, the single-particle potential in symmetric nuclear matter at ρ_0 was refitted to reproduce the empirical optical potential by Hama *et al.* [16, 17] up to nucleon kinetic energy of 1 GeV, while that in the previous MDI interaction becomes more attractive than that extracted from the proton-nucleus scattering data at nucleon momenta larger than about 550 MeV/c (i.e., the nucleon kinetic energy of about 160 MeV), as can be seen from Fig. 2 of Ref. [11]. Second, a parameter y was introduced to mimic the momentum dependence of the symmetry potential, or equivalently, the isospin splitting of the nucleon effective mass. Third, considering that the isospin tracers are sensitive to both the slope parameter L of the symmetry energy (mimiced by the parameter x in the MDI interaction) and the symmetry energy $E_{sym}(\rho_0)$ at saturation density and the constraints of the nuclear symmetry energy are usually mapped in the $L \sim E_{sym}(\rho_0)$ plane (see, e.g., Fig. 1 of Ref. [18] and Fig. 2 of Ref. [19]), a parameter z is introduced to vary the value of $E_{sym}(\rho_0)$. The ImMDI interaction can thus describe more reliably the dynamics of heavy-ion collisions at beam energies up to 1 GeV and provide possibilities to study simultaneously more detailed isovector properties of nuclear matter, such as the slope parameter of the symmetry energy, the mo-

*Electronic address: xujun@sinap.ac.cn
†Electronic address: lwchen@sjtu.edu.cn
‡Electronic address: bao-an.li@tamuc.edu

mentum dependence of the symmetry potential, and the symmetry energy at saturation density.

The neutron-proton effective mass splitting has been studied for a long time [20–24] and recently becomes again a hot topic [25–34]. It is noteworthy that in relativistic models one needs to calculate the Lorentz mass so that it can be compared with that from the non-relativistic interactions. For Lorentz effective mass, the microscopic Brueckner-Hartree-Fock or Dirac-Brueckner-Hartree-Fock approach and most Skyrme-Hartree-Fock calculations lead to a larger neutron effective mass than proton in neutron-rich nuclear matter, while most relativistic mean-field models and a few Skyrme-Hartree-Fock calculations give opposite predictions. The larger neutron effective mass than proton requires that the nuclear symmetry potential decreases with increasing nucleon momentum/energy, which is more consistent with the Lane potential in trend [22]. In addition, the neutron clearly has a larger effective mass than the proton in neutron-rich matter based on optical model analyses for nucleon-nucleus elastic scatterings [31, 32, 35]. On the other hand, the recent experimental data of double neutron/proton ratio from the National Superconducting Cyclotron Laboratory seems to favor a smaller neutron effective mass than proton based on the calculation using an improved quantum molecular dynamics model [36], although the short-range correlation might be another alternative explanation [37]. Since the possibility of a smaller neutron effective mass than proton in neutron-rich matter has not been absolutely ruled out yet and is currently hotly debated, it is thus of great interest to study in more details the possible effects from different neutron-proton effective mass splittings. It has been found that the dynamic properties in heavy-ion collisions can be affected by the isospin splitting of nucleon effective mass and the latter has considerable effects on the single and double neutron/proton ratio, t/^{3}He ratio, and isospin-dependent collective flows and particle productions [23–26, 28, 29, 33, 34]. In the present manuscript, we will study the effects on thermodynamical properties of nuclear matter from different isospin splittings of nucleon effective mass based the ImMDI interaction.

II. THE IMPROVED ISOSPIN- AND MOMENTUM-DEPENDENT INTERACTION

The functional form of potential energy density of nuclear matter for the ImMDI interaction is the same as the MDI interaction [4, 12], i.e.,

$$\begin{aligned} V(\rho,\delta) &= \frac{A_u\rho_n\rho_p}{\rho_0}+\frac{A_l}{2\rho_0}(\rho_n^2+\rho_p^2)+\frac{B}{\sigma+1}\frac{\rho^{\sigma+1}}{\rho_0^\sigma} \\ &\times (1-x\delta^2)+\frac{1}{\rho_0}\sum_{\tau,\tau'}C_{\tau,\tau'} \\ &\times \int\int d^3p d^3p' \frac{f_\tau(\vec{r},\vec{p})f_{\tau'}(\vec{r},\vec{p}')}{1+(\vec{p}-\vec{p}')^2/\Lambda^2}. \end{aligned} \quad (1)$$

In the mean-field approximation, Eq. (1) leads to the following single-particle potential [4, 12]

$$\begin{aligned} U_\tau(\rho,\delta,\vec{p}) &= A_u\frac{\rho_{-\tau}}{\rho_0}+A_l\frac{\rho_\tau}{\rho_0} \\ &+ B\left(\frac{\rho}{\rho_0}\right)^\sigma(1-x\delta^2)-4\tau x\frac{B}{\sigma+1}\frac{\rho^{\sigma-1}}{\rho_0^\sigma}\delta\rho_{-\tau} \\ &+ \frac{2C_l}{\rho_0}\int d^3p'\frac{f_\tau(\vec{r},\vec{p}')}{1+(\vec{p}-\vec{p}')^2/\Lambda^2} \\ &+ \frac{2C_u}{\rho_0}\int d^3p'\frac{f_{-\tau}(\vec{r},\vec{p}')}{1+(\vec{p}-\vec{p}')^2/\Lambda^2}. \end{aligned} \quad (2)$$

In the above, ρ_n and ρ_p are number densities of neutrons and protons, respectively, and the isospin asymmetry δ is defined as $\delta=(\rho_n-\rho_p)/\rho$, with $\rho=\rho_n+\rho_p$ being the total number density. $f_\tau(\vec{r},\vec{p})$ is the phase-space distribution function, with $\tau=1(-1)$ for neutrons (protons) being the isospin index.

The seven parameters (A_l, A_u, B, $C_l=C_{\tau,\tau}$, $C_u=C_{\tau,-\tau}$, Λ, σ) can be fitted by seven empirical constraints. Typically, five isoscalar constraints of the saturation density ρ_0, the binding energy E_0, the incompressibility K_0, the isoscalar effective mass $m_s^\star$, and the single-particle potential $U_{0,\infty}$ at infinitely large nucleon momentum at saturation density in symmetric nuclear matter can be determined by A_l+A_u, B, C_l+C_u, Λ, and σ. In addition, two isovector constraints of the symmetry energy $E_{sym}(\rho_0)$ and the symmetry potential $U_{sym,\infty}$ at infinitely large nucleon momentum (or equivalently the neutron-proton effective mass splitting) at saturation density can be determined by A_l-A_u and C_l-C_u. In addition to the x parameter in the previous MDI interaction which can be used to adjust the slope parameter L of the symmetry energy at saturation density, we introduce two addition parameters y and z to adjust respectively $U_{sym,\infty}$ and $E_{sym}(\rho_0)$, and A_l, A_u, C_l, and C_u can then be expressed as

$$A_l(x,y) = A_{l0}+y+x\frac{2B}{\sigma+1}, \quad (3)$$

$$A_u(x,y) = A_{u0}-y-x\frac{2B}{\sigma+1}, \quad (4)$$

$$C_l(y,z) = C_{l0}-2(y-2z)\frac{p_{f0}^2}{\Lambda^2\ln[(4p_{f0}^2+\Lambda^2)/\Lambda^2]}, \quad (5)$$

$$C_u(y,z) = C_{u0}+2(y-2z)\frac{p_{f0}^2}{\Lambda^2\ln[(4p_{f0}^2+\Lambda^2)/\Lambda^2]}, \quad (6)$$

where p_{f0} is the nucleon Fermi momentum in symmetric nuclear matter at saturation density. For $x=0$, $y=0$, and $z=0$, we choose the following empirical values, i.e., $\rho_0=0.16$ fm^{-3}, $E_0(\rho_0)=-16$ MeV, $K_0=230$ MeV, $m_s^\star=0.7m$, $E_{sym}(\rho_0)=32.5$ MeV, and $U_{0,\infty}=75$ MeV, which lead to $A_{l0}=A_{u0}=-66.963$ MeV, $B=141.963$ MeV, $C_{l0}=-60.4860$ MeV, $C_{u0}=-99.7017$ MeV, $\Lambda=2.42401p_{f0}$, and $\sigma=1.26521$. Again, the values of x, y, and z will only affect the isovector properties of nuclear

matter but will not lead to the variation of the empirical isoscalar constraints.

The potential energy density functional of Eq. (1) can be obtained from the following effective NN interaction within Hartree-Fock approach [4, 38]

$$v(\vec{r}_1,\vec{r}_2) = \frac{1}{6}t_3(1+x_3P_\sigma)\rho^\gamma\left(\frac{\vec{r}_1+\vec{r}_2}{2}\right)\delta(\vec{r}_1-\vec{r}_2) + (W+GP_\sigma-HP_\tau-MP_\sigma P_\tau)\frac{e^{-\mu|\vec{r}_1-\vec{r}_2|}}{|\vec{r}_1-\vec{r}_2|}, \quad (7)$$

namely, a density-dependent zero-range interaction and a finite-range Yukawa-type two-body interaction, with $\vec{r}_1$ and $\vec{r}_2$ being the spatial coordinates of the two nucleons and P_σ and P_τ being the spin and isospin exchange operator. The values of the parameters t_3, γ, W, G, H, M, and μ can be uniquely determined from A_l, A_u, B, C_l, C_u, Λ, and σ [38]. The x parameter is related to the value of x_3, i.e., the relative contribution of the isospin-singlet and the isospin-triplet channel of the density-dependent interaction, while the values of y and z are related to those of W, G, H, and M and are thus determined by the different spin-isospin channels of the finite-range interaction.

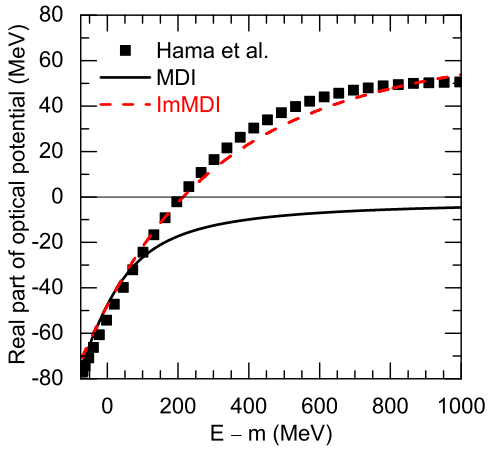

FIG. 1: (Color online) The ImMDI interaction prediction on the single-particle potential in symmetric nuclear matter at ρ_0 as a function of nucleon total energy subtracted by its rest mass. The results of the MDI interaction and the optical potential by Hama *et al.* [16, 17] are also shown for comparison.

In the ImMDI interaction, $U_{0,\infty} = (A_l + A_u)/2 + B = 75$ MeV is selected to fit the empirical optical potential by Hama *et al.*, and this can be seen from Fig. 1 where the single-particle potential (real part of optical potential) in symmetric nuclear matter at ρ_0 is plotted as a function of nucleon total energy subtracted by its rest mass, i.e., $E-m$. The results of the MDI interaction and the optical potential by Hama *et al.* [16, 17] are also shown for comparison. One can see that the MDI interaction, whose momentum dependence of the mean-field potential is fitted to reproduce that of the Gogny interaction, significantly under-predicts the empirical optical potential by Hama *et al.* when $E-m$ is larger than about 160 MeV. We note that the wrong asymptotic value of the isoscalar potential at high momentum is actually a long-standing problem of the Gogny effective interaction. On the other hand, the energy/momentum dependence of the single-particle potential in symmetric nuclear matter at ρ_0 predicted by the ImMDI interaction is in good agreement with the empirical optical potential by Hama *et al.* in the whole energy region up to about $E-m = 1000$ MeV. Therefore, the ImMDI interaction provides a reasonable choice for the transport model simulations for heavy-ion collisions at low and intermediate energies (up to at least about 1 GeV/nucleon).

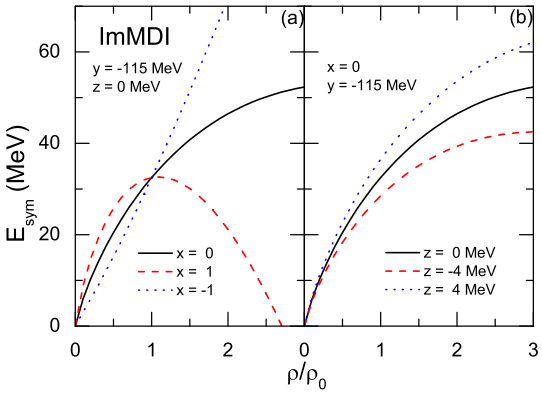

FIG. 2: (Color online) The symmetry energy from the ImMDI interaction by adjusting the value of parameter x at $y = -115$ MeV and $z = 0$ MeV (a) or parameter z at $x = 0$ and $y = -115$ MeV (b).

In the ImMDI interaction, one can vary flexibly three parameters, i.e., x, y, and z to change the isovector properties of nuclear matter. Similar to the previous MDI interaction, the density dependence of the symmetry energy (e.g., the slope parameter L) changes with the parameters x while $E_{sym}(\rho_0)$ remains unchanged, as can be seen from the left panel of Fig. 2. On the other hand, the value of the symmetry energy at saturation density changes from $E_{sym}(\rho_0)$ to $E_{sym}(\rho_0)+z$ when z is adjusted, as can be seen from the right panel of Fig. 2. In this way one can easily study the sensitivity of the isospin tracers to the values of L and $E_{sym}(\rho_0)$ simultaneously. In addition, one can vary the y parameter, which is equivalent to $U_{sym,\infty}$, to modify the momentum dependence of the symmetry potential $U_{sym}(\rho,p)$ at ρ_0 (and also other densities), while in the MDI interaction, the momentum dependence of $U_{sym}(\rho,p)$ is fixed although the magnitude of $U_{sym}(\rho,p)$ at non-saturation densities can be varied using different x values. It is clearly seen from the left panel of Fig. 3 that one can flexibly vary y parameter to mimic different momentum/energy dependences of the

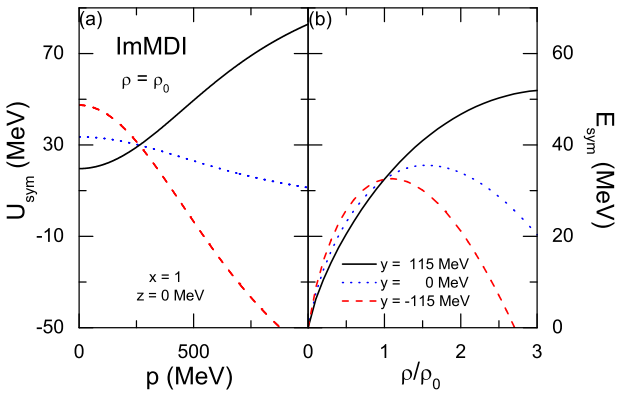

FIG. 3: (Color online) The symmetry potential at saturation density (a) and symmetry energy (b) from the ImMDI interaction by adjusting the value of parameter y at $x = 1$ and $z = 0$ MeV.

$U_{sym}(\rho, p)$ (and thus isospin splitting of nucleon effective mass), providing a convenient way to explore the consequent effects in heavy-ion collisions. In addition, one can see $U_{sym}(\rho_0, p)$ at $p = p_{f0}$ (corresponding to a nucleon kinetic energy of 36.8 MeV) is independent of the y parameter by construction. On the other hand, it is seen from the right panel of Fig. 3 that the density dependence of the symmetry energy changes with y as well, with the values of $E_{sym}(\rho_0)$ fixed. This can be understood as the slope parameter L depends on not only the magnitude of symmetry potential, which is related to the x parameter, but also the momentum dependence of the symmetry potential [35, 39].

III. EFFECTS OF NEUTRON-PROTON EFFECTIVE MASS SPLITTING

The ImMDI interaction described in the previous section provides possibilities of studying more detailed isovector properties of nuclear matter flexibly. In the following, we study the effects of neutron-proton effective mass splitting on thermodynamical properties of neutron-rich nuclear matter. One can see from Figs. 2 and 3 that $[(x = 0), (y = -115$ MeV$)]$ and $[(x = 1), (y = 115$ MeV$)]$ give almost the same density dependence of the symmetry energy at $z = 0$, while the two parameter sets lead to two extreme momentum dependences of the symmetry potential, with U_{sym} from $[(x = 0), (y = -115$ MeV$)]$ decreases with increasing nucleon momentum and thus $m_n^\star > m_p^\star$ and that from $[(x = 1), (y = 115$ MeV$)]$ increases with increasing nucleon momentum and thus $m_n^\star < m_p^\star$. We will carry out our study based on the two parameter sets in the following.

A. temperature dependence of symmetry energy

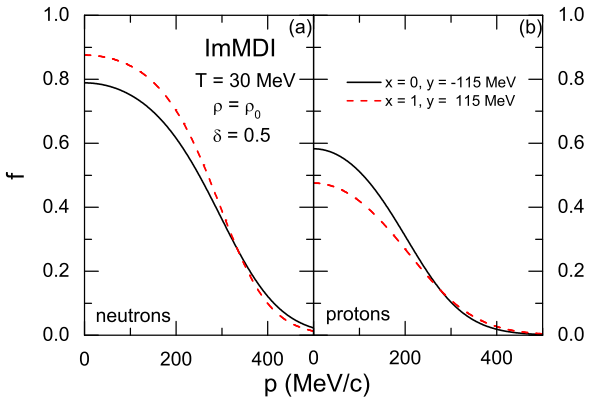

FIG. 4: (Color online) The equilibrated phase-space distribution functions (normalized by the spin degeneracy) of neutrons (a) and protons (b) from the ImMDI interaction for $[(x = 0), (y = -115$ MeV$)]$ and $[(x = 1), (y = 115$ MeV$)]$ in neutron-rich nuclear matter of isospin asymmetry $\delta = 0.5$ at saturation density and temperature $T = 30$ MeV.

Since from Eq. (2) the single-particle potential depends on the phase-space distribution function, and from single particle approximation this Fermi-Dirac phase-space distribution function in equilibrium depends on the single-particle potential, an iteration method is needed to calculate the mean-field potential and the equation of state at finite temperatures [40]. From such a self-consistent calculation, the equilibrated phase-space distribution functions of neutrons and protons for $[(x = 0), (y = -115$ MeV$)]$ and $[(x = 1), (y = 115$ MeV$)]$ in neutron-rich nuclear matter of isospin asymmetry $\delta = 0.5$ at saturation density and temperature $T = 30$ MeV are displayed in Fig. 4. It is seen that $[(x = 0), (y = -115$ MeV$)]$, giving a larger neutron effective mass than proton, has a more diffusive distribution for neutrons and less diffusive distribution for protons compared to $[(x = 1), (y = 115$ MeV$)]$. This is understandable as the self-consistent calculation balances the energy of the system at fixed isospin asymmetry, so for a larger neutron (proton) effective mass than proton (neutron) with $[(x = 0), (y = -115$ MeV$)]$ ($[(x = 1), (y = 115$ MeV$)]$) more neutrons (protons) are allowed to occupy the high-momentum states.

As a key quantity of isospin physics, the density dependence of the symmetry energy for $[(x = 0), (y = -115$ MeV$)]$ and $[(x = 1), (y = 115$ MeV$)]$ at different temperatures are shown in Fig. 5. At finite temperatures the symmetry energy is calculated numerically by taking the difference of the binding energy at $\delta = 0$ and $\delta = 0.2$. One can see for $[(x = 0), (y = -115$ MeV$)]$ the symmetry energy decreases with increasing temperature at lower densities but slightly increases with increasing temperature at higher densities, while for $[(x = 1), (y = 115$ MeV$)]$ the symmetry energy decreases with

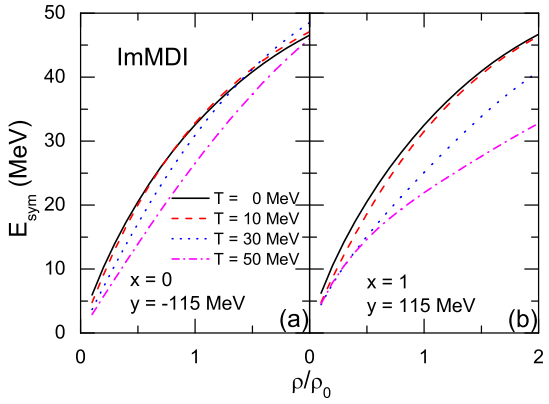

FIG. 5: (Color online) The nuclear symmetry energy from the ImMDI interaction for [$(x = 0)$, $(y = -115$ MeV)] (a) and [$(x = 1)$, $(y = 115$ MeV)] (b) at temperatures of 0, 10, 30, and 50 MeV.

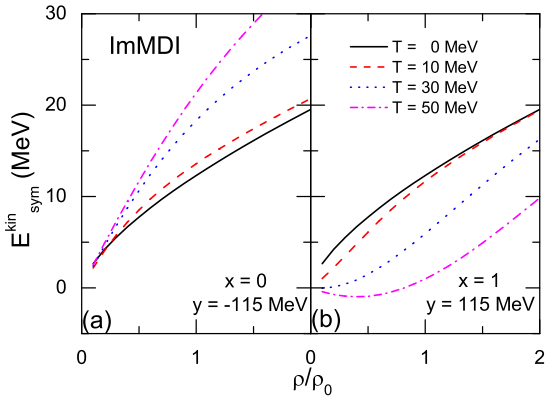

FIG. 6: (Color online) Same as Fig. 5 but only for the kinetic contribution of the symmetry energy.

increasing temperature at all the densities. Similar behavior was observed in Ref. [26] based on the Skyrme-Hartree-Fock functional. To understand the different temperature dependence of the symmetry energy with different isospin splitting of nucleon effective mass, we further show in Figs. 6 and 7 the kinetic and potential contribution to the symmetry energy, respectively. It is interesting to see that the kinetic contribution to the symmetry energy increases with increasing temperature for $[(x = 0)$, $(y = -115$ MeV$)]$ but decreases with increasing temperature for $[(x = 1)$, $(y = 115$ MeV$)]$. This is because there are more neutrons and less protons in the high-energy states with increasing temperature for $[(x = 0)$, $(y = -115$ MeV$)]$ but it is opposite for $[(x = 1)$, $(y = 115$ MeV$)]$, as can be seen from Fig. 4. For the potential contribution to the symmetry energy, it somehow decreases with increasing temperature for $[(x = 0)$, $(y = -115$ MeV$)]$ but has a weak temperature dependence for $[(x = 1)$, $(y = 115$ MeV$)]$. The combination of Figs. 6 and 7 leads to the temperature dependence of the total symmetry energy in Fig. 5.

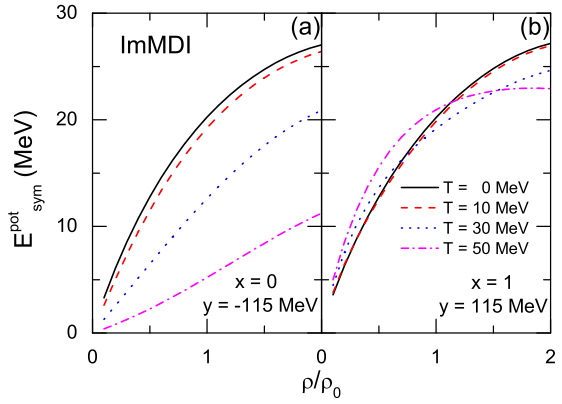

FIG. 7: (Color online) Same as Fig. 5 but only for the potential contribution of the symmetry energy.

B. isovector single-particle properties

We now move to the isovector single-particle properties of nuclear matter including the symmetry potential and the neutron-proton effective mass splitting. The momentum dependence of the symmetry potential for $[(x = 0)$, $(y = -115$ MeV$)]$ and $[(x = 1)$, $(y = 115$ MeV$)]$ at different densities and temperatures are shown in Fig. 8, and the results are calculated by taking the potential difference of neutrons and protons at $\delta = 0.2$. One can see that the symmetry potential decreases with increasing momentum for $[(x = 0)$, $(y = -115$ MeV$)]$ but increases with increasing momentum for $[(x = 1)$, $(y = 115$ MeV$)]$, and the slope is larger at higher densities. The symmetry potential becomes negative at high nucleon momenta for $[(x = 0)$, $(y = -115$ MeV$)]$ while it is always positive for $[(x = 1)$, $(y = 115$ MeV$)]$. With the increasing temperature, only the low-momentum part of the symmetry potential is affected while the high-momentum part remains almost unchanged. It is interesting to see that symmetry potential decreases with increasing temperature for $[(x = 0)$, $(y = -115$ MeV$)]$ while it increases with increasing temperature for $[(x = 1)$, $(y = 115$ MeV$)]$.

A positive symmetry potential gives repulsive force to neutrons and attractive force to protons, while the velocity of the nucleon depends not only on the force but also on the in-medium effective mass. The nucleon effective mass, which is defined as

$$\frac{m^*_\tau}{m} = \left(1 + \frac{m}{p}\frac{dU_\tau}{dp}\right)^{-1}, \tag{8}$$

is a function of nucleon momentum but mostly represented by the value at Fermi momentum. The relative neutron-proton effective mass splitting for $[(x = 0)$,

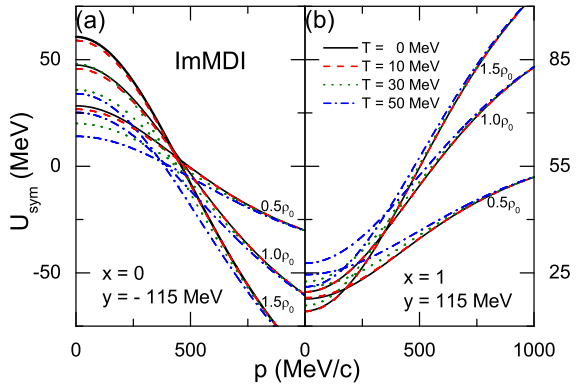

FIG. 8: (Color online) The momentum dependence of the symmetry potential from the ImMDI interaction for [$(x = 0)$, $(y = -115$ MeV$)$] (a) and [$(x = 1)$, $(y = 115$ MeV$)$] (b) at different densities and temperatures.

$(y = -115$ MeV$)$] and [$(x = 1)$, $(y = 115$ MeV$)$] in neutron-rich nuclear matter of isospin asymmetry $\delta = 0.5$ at different densities and temperatures are shown in Fig. 9. Indeed, the neutron effective mass is larger than protons for [$(x = 0)$, $(y = -115$ MeV$)$] and smaller than protons for [$(x = 1)$, $(y = 115$ MeV$)$] at all the densities and temperatures. Generally, the relative effective mass splitting is smaller at higher nucleon momenta and stronger at higher densities, and the splitting becomes weaker at higher temperatures for [$(x = 0)$, $(y = -115$ MeV$)$] but the temperature dependence is somehow complicated for [$(x = 1)$, $(y = 115$ MeV$)$] especially at higher densities.

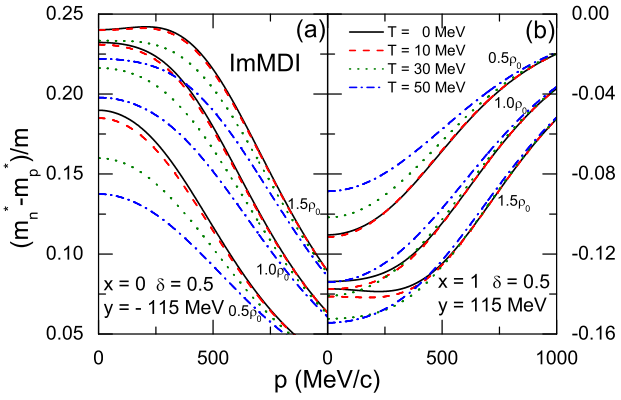

FIG. 9: (Color online) The relative neutron-proton effective mass splitting from the ImMDI interaction for [$(x = 0)$, $(y = -115$ MeV$)$] (a) and [$(x = 1)$, $(y = 115$ MeV$)$] (b) in neutron-rich nuclear matter of isospin asymmetry $\delta = 0.5$ at different densities and temperatures.

C. differential isospin fractionation

The two phases of nuclear matter can coexist if the Gibbs condition is satisfied, i.e., they have the same temperature, pressure, and chemical potential. The dense phase with smaller isospin asymmetry is called the liquid phase, while the dilute phase with larger isospin asymmetry is called the gas phase. As the symmetry energy generally increases with increasing density at least at subsaturation densities, the high-density phase should have a smaller isospin asymmetry while the low-density phase can have a larger isospin asymmetry, so in this way the total energy can be well distributed in the two phases and reach a minimum value. This is the so-called isospin fractionation.

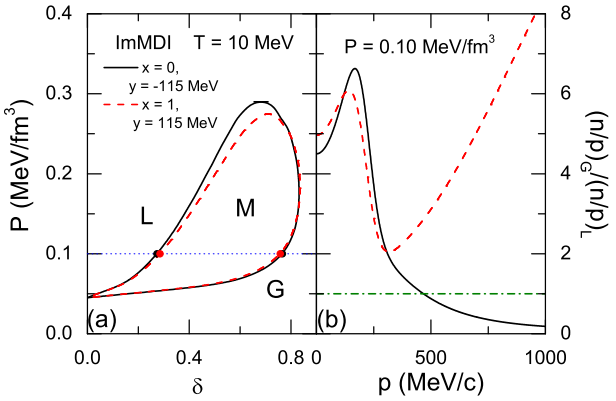

FIG. 10: (Color online) Left panel: The section of binodal surface from the ImMDI interaction for [$(x = 0)$, $(y = -115$ MeV$)$] and [$(x = 1)$, $(y = 115$ MeV$)$] at a temperature $T = 10$ MeV, and L, G, and M represent the liquid phase, the gas phase, and the mixed phase, respectively; Right panel: The double neutron/proton ratio in gas and liquid phases $(n/p)_G/(n/p)_L$ at the pressure of 0.10 MeV/fm^3 as a function of nucleon momentum.

Numerically, the binodal surface of nuclear liquid-gas phase transition can be constructed by drawing rectangles in the chemical potential isobars of neutrons and protons as functions of isospin asymmetry at a given temperature [41, 42]. The obtained two phases thus satisfy the Gibbs condition, with the one of larger isospin asymmetry corresponding to the gas phase and that of the smaller isospin asymmetry corresponding to the liquid phase. Collecting all such pairs at each pressure forms the binodal surface of the nuclear liquid-gas phase transition, as shown in the left panel of Fig. 10 at temperature $T = 10$ MeV. The binodal surface is useful in calculating the volume fraction of each phase and studying the properties of nuclear liquid-gas phase transition at fixed isospin asymmetry as shown in Ref. [7], and the liquid phase (L), the gas phase (G), and the mixed phase (M) are denoted in the figure. One can see that the binodal surface is similar for [$(x = 0)$, $(y = -115$ MeV$)$] and

[$(x = 1)$, $(y = 115$ MeV)]. This is not surprising as both the chemical potential and the pressure are determined from the equation of state, which is almost the same for the two parameter sets. The slight difference is expected to be due to the different temperature dependence of the symmetry energy.

Similar to Ref. [43], we study the differential isospin fractionation at pressure $P = 0.1$ MeV/fm^3. As can be seen from the left panel of Fig. 10, the nuclear matter in the mixed phase region at $P = 0.1$ MeV/fm^3 composes of the liquid phase and the gas phase at two edges of the binodal surface with the same pressure. For [$(x = 0)$, $(y = -115$ MeV)], the densities and isospin asymmetries of the liquid and gas phases are $\rho_L = 0.757\rho_0$, $\delta_L = 0.273$, $\rho_G = 0.087\rho_0$, and $\delta_G = 0.766$, respectively. For [$(x = 1)$, $(y = 115$ MeV)], the densities and isospin asymmetries of the liquid and gas phases are $\rho_L = 0.752\rho_0$, $\delta_L = 0.285$, $\rho_G = 0.083\rho_0$, and $\delta_G = 0.758$, respectively. Thus, the ratios of neutron/proton in the gas phase to that in the liquid phase, i.e, $(n/p)_G/(n/p)_L$, are 4.31 for [$(x = 0)$, $(y = -115$ MeV)] and 4.04 for [$(x = 1)$, $(y = 115$ MeV)]. Although the total ratios are similar for the two parameter sets, the differential behaviors, i.e., the momentum dependence, are quite different, as can be seen from the right panel of Fig. 10. Similar to the findings in Ref. [43], the $(n/p)_G/(n/p)_L$ ratio becomes smaller than 1 when the nucleon momentum is larger than about 500 MeV/c. This can be understood by checking with the symmetry potential in Fig. 8 that U_{sym} becomes negative when the nucleon momentum is larger than about 500 MeV/c. For [$(x = 1)$, $(y = 115$ MeV)], since the symmetry potential is always positive and is larger at higher nucleon momenta, the $(n/p)_G/(n/p)_L$ ratio is always larger than 1 and increases with increasing momentum at higher nucleon energies. In intermediate-energy heavy-ion collisions, the gas phase is formed by free nucleons while the liquid phase is formed by those in heavy clusters. Consistent with the finding here, it was show in Refs. [23, 24, 29, 33] that the neutron/proton ratio of energetic nucleons is sensitive to the neutron-proton effective mass splitting.

IV. SUMMARY

Based on an improved isospin- and momentum-dependent interaction, with the isoscalar single-nucleon potential refitted to that extracted by optical model analyses of proton-nucleus scattering data up to nucleon kinetic energy of about 1 GeV/c, and three parameters included for studing the detailed isovector properties of nuclear matter, i.e., the slope parameter of the symmetry energy, the momentum dependence of the symmetry potential, and the symmetry energy at saturation density, we have studied the thermodynamical properties of neutron-rich nuclear matter with the same equation of state but different neutron-proton effective mass splittings. We found that the phase-space distribution in equilibrium, the temperature dependence of the symmetry energy, and the differential isospin fractionation can be affected by the isospin splitting of nucleon effective mass.

V. ACKNOWLEDGMENTS

This work was supported in part by the Major State Basic Research Development Program (973 program) in China under Contract Nos. 2015CB856904, 2014CB845401, and 2013CB834405, the National Natural Science Foundation of China under Grant Nos. 11475243, 11275125, 11135011, and 11320101004, the "100-talent plan" of Shanghai Institute of Applied Physics under Grant No. Y290061011 from the Chinese Academy of Sciences, the "Shanghai Pujiang Program" under Grant No. 13PJ1410600, the Shu Guang project supported by Shanghai Municipal Education Commission and Shanghai Education Development Foundation, the Program for Professor of Special Appointment (Eastern Scholar) at Shanghai Institutions of Higher Learning, the Science and Technology Commission of Shanghai Municipality (11DZ2260700), the US National Science Foundation grants PHY-1068022, the National Aeronautics and Space Administration under grant NNX11AC41G issued through the Science Mission Directorate, and the CUSTIPEN (China-U.S. Theory Institute for Physics with Exotic Nuclei) under DOE grant number DE-FG02-13ER42025.

[1] C. Gale, G. Bertsch, and S. Das Gupta, Phys. Rev. C **35**, 1666 (1987).
[2] G.M. Welke *et al.*, Phys. Rev. C **38**, 2101 (1988).
[3] C. Gale *et al.*, Phys. Rev. C **41**, 1545 (1990).
[4] C.B. Das, S. Das Gupta, C. Gale, and B.A. Li, Phys. Rev. C **67**, 034611 (2003).
[5] B.A. Li, L.W. Chen, and C.M. Ko, Phys. Rep. **646**, 113 (2008).
[6] V. K. Mishra, G. Fai, L. P. Csernai, and E. Osnes, Phys. Rev. C**47**, 1519 (1993).
[7] J. Xu, L.W. Chen, B.A. Li, and H.R. Ma, Phys. Rev. C **77**, 014302 (2008).
[8] J. Xu, L.W. Chen, B.A. Li, and H.R. Ma, Phys. Rev. C **79**, 035802 (2009).
[9] J. Xu, L.W. Chen, B.A. Li, and H.R. Ma, Astro. Phys. J. **697**, 1549 (2009).
[10] J. Xu, L.W. Chen, C.M. Ko, and B.A. Li, Phys. Rev. C **81**, 055805 (2010).

[11] J. Xu, L.W. Chen, C.M. Ko, and B.A. Li, Phys. Rev. C **81**, 055803 (2010).
[12] L.W. Chen, C.M. Ko, and B.A. Li, Phys. Rev. Lett. **94**, 032701 (2005).
[13] Z.G. Xiao, B.A. Li, L.W. Chen, G.C. Yong, and M. Zhang, Phys. Rev. Lett. **102**, 062502 (2009).
[14] L.W. Chen, C.M. Ko, B.A. Li, C. Xu, and J. Xu, Eur. Phys. J. A **50**, 29 (2014).
[15] L.W. Chen and B.A. Li, A note of an improved MDI interaction for transport model simulations of heavy ion collisions (Unpublished, Texas A&M University-Commerce, 2010).
[16] S. Hama *et al.*, Phys. Rev. C **41**, 2737 (1990).
[17] E.D. Cooper, S. Hama, B.C. Clark, and R.L. Mercer, Phys. Rev. C **47**, 297 (1993).
[18] L.W. Chen, arXiv: 1212.0284 [nucl-th].
[19] M.B. Tsang *et al.*, arXiv: 1204.0466 [nucl-ex]
[20] B. Liu *et al.*, Phys. Rev. C **65**, 045201 (2002).
[21] Z.Y. Ma *et al.*, Phys. Lett. B **604**, 170 (2004).
[22] B.A. Li, Phys. Rev. C **69**, 064602 (2004).
[23] B.A. Li, C.B. Das, S. Das Gupta, and C. Gale, Phys. Rev. C **69**, 011603 (2004); *ibid*, Nucl. Phys. A **735**, 563 (2004).
[24] J. Rizzo, M. Colonna, and M. Di Toro, Phys. Rev. C **72**, 064609 (2005).
[25] V. Giordano *et al.*, Phys. Rev. C **81**, 044611 (2010).
[26] L. Ou *et al.*, Phys. Lett. B **697**, 246 (2011).
[27] B. Behera, T.R. Routray, and S.K. Tripathy, J. Phys. G: Nucl. Part. Phys. **38**, 115104 (2011).
[28] Z.Q. Feng, Phys. Rev. C **84**, 024610 (2011).
[29] Z.Q. Feng, Nucl. Phys. A **878**, 3 (2012).
[30] B.A. Li and X. Han, Phys. Lett. B **272**, 276 (2013).
[31] X.H. Li *et al.*, Phys. Lett. B **721**, 101 (2013).
[32] X.H. Li *et al.*, arXiv: 1403.5577 [nucl-th].
[33] Y.X. Zhang, M.B. Tsang, Z.X. Li, and H. Liu, Phys. Lett. B **732**, 186 (2014).
[34] W.J. Xie and F.S. Zhang, Phys. Lett. B **735**, 250 (2014).
[35] C. Xu, B.A. Li, and L.W. Chen, Phys. Rev. C **82**, 054607 (2010).
[36] D.D.S. Coupland *et al.*, arXiv: 1406.4546 [nucl-th].
[37] O. Hen *et al.*, arXiv: 1408.0772 [nucl-th], Phys. Rev. C in press.
[38] J. Xu and C.M. Ko, Phys. Rev. C **82**, 044311 (2010).
[39] R. Chen *et al.*, Phys. Rev. C **85**, 024305 (2012).
[40] J. Xu, L.W. Chen, B.A. Li, and H.R. Ma, Phys. Rev. C **75**, 014607 (2007).
[41] H. Müller and B.D. Serot, Phys. Rev. C **52**, 2072 (1995).
[42] J. Xu, L.W. Chen, B.A. Li, and H.R. Ma, Phys. Lett. B **650**, 348 (2007).
[43] B.A. Li, L.W. Chen, H.R. Ma, J. Xu, and G.C. Yong, Phys. Rev. C **76**, 051601(R) (2007).